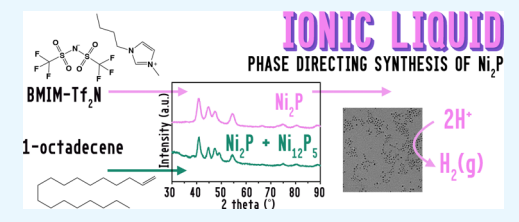
Phase Directing Ability of an Ionic Liquid Solvent for the Synthesis of HER-Active Ni₂P Nanocrystals

Emily J. Roberts, Carlos G. Read, Nathan S. Lewis, 4, 0 and Richard L. Brutchey, 10

Supporting Information

ABSTRACT: An ionic liquid (IL) solvent was used to synthesize small, phase-pure nickel phosphide (Ni₂P) nanocrystals. In contrast, under analogous reaction conditions, substitution of the IL for the common high-boiling organic solvent 1-octadecene (ODE) results in phase-impure nanocrystals. The 5 nm Ni₂P nanocrystals prepared in IL were electrocatalytically active toward the hydrogen evolution reaction. The synthesis in IL was also extended to alloyed Ni_{2-x}Co_xP nanocrystals, where $0.5 \le x \le 1.5$.



KEYWORDS: ionic liquid, nickel phosphide, nanocrystal, electrocatalyst, hydrogen evolution reaction

Room temperature ionic liquids (ILs) have garnered increased interest because of their unique physicochemical properties relative to those of traditional organic solvents. For example, ILs are nonflammable, have high thermal and chemical stability, possess a wide liquidus range, and have extremely low vapor pressures ($\sim 10^{-10}$ Pa at 25 °C), among other properties that result in environmental health and safety benefits relative to traditional organic solvents. 1,2 As a result of these unique properties, ILs are becoming an increasingly attractive class of solvents for the synthesis of colloidal inorganic nanocrystals.

The low interfacial tension possessed by ILs tends to induce rapid nucleation rates, resulting in small particles with high surface-area-to-volume ratios.² In addition, ILs can stabilize the surfaces of inorganic nanocrystals through combined electrostatic and steric effects, minimizing agglomeration and Ostwald ripening.² Consequently, imidazolium-based ILs have been investigated as dual-functioning solvents and stabilizers for the synthesis of a variety of colloidal inorganic nanocrystals, including metal and metal oxide nanocrystals (e.g., Au, Ag, Pt, Rh, Cu, ZnO, NiO, TiO₂, and Fe₃O₄).³⁻⁸ Despite the reported thermal stability of many ILs, their practical utilization in high-temperature colloidal nanocrystal syntheses is not welldeveloped.

We report herein the high-temperature synthesis of Ni₂P nanocrystals as an interesting proof-of-concept reaction. Ni₂P has attracted considerable interest as a result of the relative Earth abundance of its constituent elements, stability in alkaline as well as acidic media, and catalytic activity for the hydrodeoxygenation of biomass, the hydrodesulfurization of petrol, and the hydrogen evolution reaction (HER). 9-11 The binary Ni-P phase diagram is complex, with a large number of thermodynamically stable stoichiometries (Ni₃P, Ni₅P₂, Ni₁₂P₅, Ni₂P, Ni₅P₄, NiP, NiP₂, and NiP₃), thereby creating a synthetic challenge with respect to accessing phase-pure Ni₂P. In general, increasing the molar equivalents of the phosphide precursor,

extending the reaction time, and operating at higher temperatures allow the more phosphorus-rich side of the phase diagram to be accessed for colloidal nanocrystals. 12-14

Typical methods used to synthesize high-quality colloidal Ni₂P nanocrystals use traditional organic solvents (e.g., octadecene (ODE), dioctyl ether), expensive and/or reactive phosphide precursors (tri-n-octylphosphine (TOP), white phosphorus (P_4) , tris(trimethylsilyl)phosphine $(P(TMS)_3)$, and tri-*n*-butylphosphine), high temperatures, and/or multiple-step reactions. ^{10,15–17} Triphenylphosphine (PPh₃) is a lowcost, less-reactive, and more air-stable phosphide precursor (~15% the cost of TOP in price per mole);¹⁸ however, compared to those with TOP and P(TMS)3, nanocrystals synthesized using PPh3 are typically large (>45 nm), ill-defined, amorphous, and/or not phase pure. 18-

Herein, we report the one-step, heating up synthesis of Ni₂P nanocrystals using $Ni(acac)_2$, PPh_3 , oleylamine (OAm), and 1butyl-3-methylimidazolium bis(trifluoromethylsulfonyl)imide (BMIM-Tf₂N) as the IL solvent (eq 1, see Supporting Information for detailed experimental section). This particular IL solvent was specifically chosen for its superior thermal stability, because weakly coordinating anions are relatively stable with respect to high-temperature decomposition. The ~12 mol equiv of PPh3 was used since lower P:Ni precursor ratios resulted in larger, phase-impure nanocrystals. When the reactants were heated to 310 °C at a rate of ~10 °C min⁻¹ and held at temperature for 30 min, small, phase-pure Ni₂P nanocrystals were obtained. The isolated yield of the resulting Ni₂P nanocrystals was 80% relative to the Ni(acac)₂ precursor, as assessed by organic content-corrected thermogravimetric analysis (Figure S1).

Received: February 13, 2018 Accepted: May 3, 2018 Published: May 3, 2018



Department of Chemistry, University of Southern California, Los Angeles, California 90089, United States

[‡]Division of Chemistry and Chemical Engineering, California Institute of Technology, Pasadena, California 91125, United States

ACS Applied Energy Materials

$$Ni(acac)_2 + 12 \text{ equiv PPh}_3 \xrightarrow[310 {}^{\circ}\text{C}, 30 \text{ min}]{} Ni_2P$$
 (1)

All of the diffraction peaks in the powder X-ray diffraction (XRD) pattern of the resulting nanocrystals were ascribable to the hexagonal structure of Ni₂P (Figure 1a), indicating that the

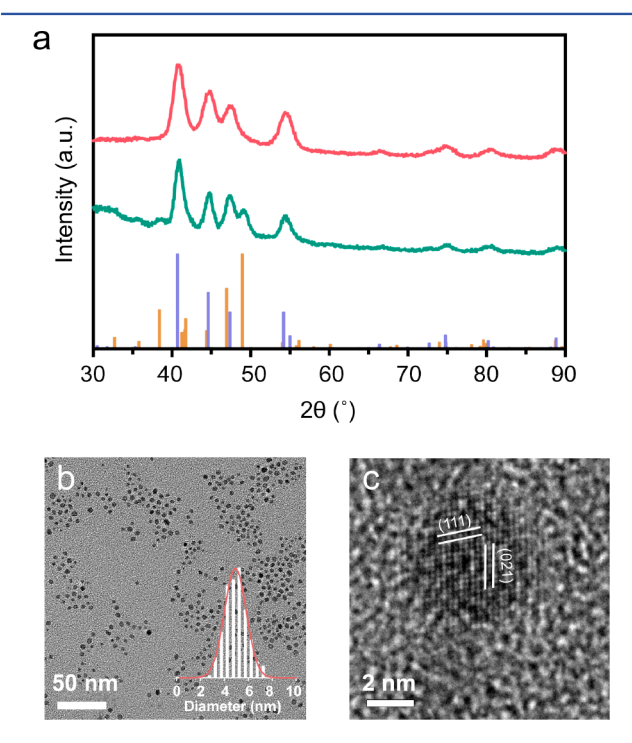


Figure 1. (a) XRD patterns of nickel phosphide nanocrystals synthesized in BMIM-Tf₂N (red) and 1-octadecene (green) at 310 $^{\circ}$ C for 30 min. The purple stick pattern represents Ni₂P, and the gold stick pattern represents Ni₁₂P₅. (b) TEM micrograph and corresponding size histogram (inset) of Ni₂P nanocrystals synthesized in BMIM-Tf₂N. (c) High-resolution TEM micrograph displaying lattice fringes of the (111) and (021) planes.

resulting product was crystalline and phase-pure Ni₂P. The diffraction peaks at 40.87°, 44.79°, 47.60°, and 54.44° 2θ can be indexed to the (111), (021), (210), and (002) reflections, respectively. The lattice parameters were calculated to be a =5.85 and c = 3.37 nm, which are in good agreement with those reported for bulk Ni₂P (PDF 01-089-2742). Scherrer analysis of the peak broadening yielded an average grain size of 5.6 nm. Transmission electron microscope (TEM) images revealed that the resulting Ni₂P nanocrystals were spherical in shape, with an average diameter of 5.0 ± 0.9 nm, and a standard deviation about the mean (σ/d) of 18%. The nanocrystal size is in agreement with the predicted grain size determined by Scherrer analysis, consistent with the formation of single-domain particles (Figure 1b,c). No void spaces within the nanocrystals were observable by high-resolution TEM analysis (Figure 1c), implying that the growth mechanism may not involve the phosphidation of a crystalline Ni intermediate, which typically results in particle hollowing by the Kirkendall effect. 21 A dspacing of 0.220 and 0.204 nm was calculated for the observed lattice fringes, corresponding to the (111) and (021) planes of the hexagonal Ni₂P structure, respectively.

When ODE was substituted in place of BMIM-Tf₂N as the solvent, under otherwise identical reaction conditions, mixed-phased products were obtained after 30 min at 310 $^{\circ}$ C. These products contained the phosphorus-poor Ni₁₂P₅ phase as well

as the desired Ni₂P phase, as indicated by the presence of an additional diffraction peak at ${\sim}49^{\circ}~2\theta$ by XRD that corresponds to the 100% intensity (312) reflection of Ni₁₂P₅ (PDF 01-089-2742) (Figure 1a). TEM micrographs revealed that the phase-impure nanocrystals synthesized in ODE were relatively ill-defined and faceted, with the particles having almost twice the average diameter (10.9 \pm 2.5 nm; σ/d = 23%) as those synthesized by the analogous reaction in IL (Figure S2). The relatively smaller size of the resulting nanocrystals synthesized in BMIM-Tf₂N suggests that the IL is playing an important role during synthesis, consistent with expectations that ILs can provide shape 22,23 and size-directing $^{23-25}$ capabilities, but this is the first report of obtaining a specific phase by using an IL solvent instead of traditional organic solvents.

A variable temperature study was performed to understand in more detail the phase evolution that occurred in BMIM- Tf_2N relative to ODE as the solvent (Figure 2). In BMIM- Tf_2N ,

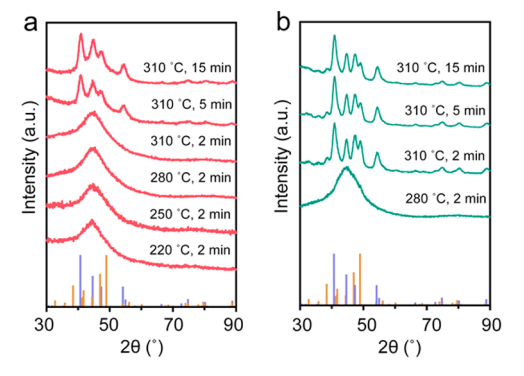


Figure 2. Powder XRD patterns of nickel phosphide nanocrystal syntheses performed at various times and temperatures in (a) BMIM- Tf_2N and (b) ODE solvents. The purple stick pattern corresponds to Ni_1P , and the gold stick pattern corresponds to Ni_1P_5 .

nucleation was observed beginning at ~180 °C, and isolable particles were produced by 220 °C, which is also the temperature at which significant phosphine gas evolution is observed. 12 In the absence of OAm, no nucleation is observed, indicating that OAm is acting as the primary reducing agent. When the same molar equivalents of TOP were substituted for PPh₃, the particles were not isolatable due to their small size. For all temperatures up to 310 °C, powder XRD patterns of the reaction products displayed a single broad peak that has previously been assigned to an amorphous Ni-P phase.²⁶ This diffraction peak is in agreement with Brock's observation of the formation of an amorphous Ni-P phase when higher P:Ni stoichiometric ratios are used. 13 In contrast, when ODE is substituted as the solvent, nucleation was not observed until 200-220 °C. Postnucleation, nuclei were not isolable in ODE at temperatures below 280 °C due to their small size. Moreover, gas evolution is not observed in ODE until ~260 °C. Hence, both particle nucleation and phosphine gas evolution occurred at lower temperatures in the IL solvent than when in ODE. The diffractogram for the reaction product from ODE at 280 $^{\circ}\text{C}$ displayed a similar amorphous Ni–P phase as the particles obtained from the IL solvent, but exhibited a significant shoulder at 49° 2θ , which can be indexed to the 100% intensity peak of Ni₁₂P₅. In ODE, once the reaction temperature reached 310 °C for 2 min, a mixed-phase Ni₁₂P₅-Ni₂P product was obtained, and it has previously been reported that crystalline Ni₁₂P₅ can serve as an intermediate **ACS Applied Energy Materials**

phase to Ni₂P in ODE.²⁷ The data are thus consistent with the hypothesis that evolution of the Ni₂P phase in the IL solvent does not proceed through an observable Ni₁₂P₅ intermediate, as is observed in ODE, but rather has a delayed amorphous-to-crystalline transition that leads directly to the crystalline, more phosphorus-rich phase; however, obtaining a high yield required a reaction time of 30 min. These results imply that the IL may be interacting with the surface and consequently influencing nucleation and growth.

To determine if the IL was coordinated to the purified nanocrystal surface, high-resolution X-ray photoelectron spectroscopic (XPS) data were collected showing F 1s and S 2p signals, confirming the presence of the Tf_2N^- anion (Figure S3a,b). Three sets of doublets were observed in the Ni 2p region, with the first set of $2p_{3/2}$ and $2p_{1/2}$ peaks having binding energies of 852.9 and 870.2 eV, respectively, and possessing the expected spin—orbit splitting ($\Delta = 17.3$ eV) for Ni species (Figure 3a). The observed Ni $2p_{3/2}$ binding energy is slightly

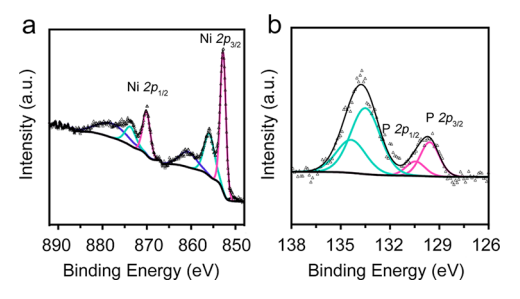


Figure 3. High-resolution XPS spectra of (a) Ni 2p and (b) P 2p regions.

higher than that of metallic Ni (Ni 0 2p_{3/2} = 852.7 eV), consistent with a Ni $^{\delta+}$ species that is in good agreement with previous reports for Ni₂P. The remaining doublets, with 2p_{3/2} binding energies of 855.8 and 861.0 eV, can be assigned to oxidized surface species (e.g., NiO and NiOOH) and expected satellite peaks, respectively.

The high-resolution XPS data in the P 2p region exhibited peak envelopes at binding energies of 130.2 and 134.2 eV, each of which consisted of doublets with $2p_{3/2}$ peaks at 129.8 and 134.0 eV, respectively (Figure 3b). Both doublets exhibited the expected spin—orbit splitting of 0.8 eV. The peak present at lower binding energies can be attributed to reduced P species within the Ni₂P structure, while the doublet at ~134 eV is ascribable to oxidized P⁵⁺ surface species.³⁰ The surface oxidation of both Ni and P is a result of storage in air and is not expected to deleteriously influence the catalytic activity of the Ni₂P nanocrystals, provided that the material is reduced prior to catalysis (vide infra).

To further confirm the presence of BMIM-Tf₂N on the surface of the nanocrystals, FT-IR spectra of the Ni₂P nanocrystals were obtained postpurification (Figure S4). Symmetric and asymmetric $\nu(SO_2)$ stretching bands at 1135 and 1350 cm⁻¹, and an asymmetric $\nu(CF_3)$ stretching band at 1196 cm⁻¹, correspond to the presence of the Tf₂N⁻ anion and corroborate the XPS observations. Bands from the overlapping modes of the BMIM⁺ cation, including $\nu(C-C)$ and $\nu(NCH_3)$, appear at 1055 cm⁻¹, in a region where both OAm and PPh₃ do not exhibit IR-active modes.³¹ Additionally, PPh₃ or oxidized Ph₃P=O species are likely coordinated to the nanocrystal surface, as indicated by the appearance of bands appearing at 1436, 1477, and 1581 cm⁻¹ that are ascribable to phenyl C-C

bond stretches.³² No IR bands expected for coordinated OAm were observed in the Ni₂P nanocrystals. The observation of FT-IR bands corresponding to BMIM-Tf₂N is consistent with the IL acting as a stabilizer.²² Coordination to the surface thus appears to influence the resulting phase and morphology, and supports the observation of small, single-phase particles as compared to the nanocrystals produced in noncoordinating ODE under analogous conditions.

The HER activity of the Ni_2P nanocrystals was also evaluated and compared to Ni_2P nanocrystals that were synthesized by more conventional routes. The working electrode was prepared by drop-casting a colloidal suspension of purified Ni_2P nanocrystals onto a Ti foil substrate (to achieve a mass loading ~ 1 mg cm⁻²), followed by heating at 400 °C in forming gas (5% $H_2/95\%$ N_2) for 1 h to remove ligands and reduce any oxidized surface species. ¹⁰ A typical three-electrode setup in 0.5 M $H_2SO_4(aq)$ was utilized. Figure 4a presents the polarization

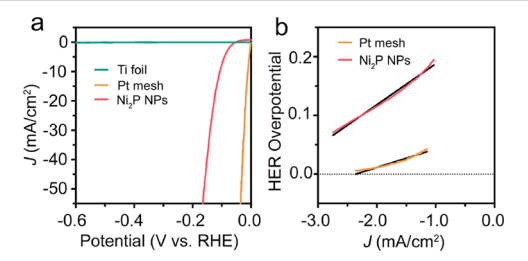


Figure 4. (a) Polarization data in 0.5 M H_2SO_4 for Ni_2P nanocrystals synthesized in BMIM- Tf_2N on a Ti foil substrate, bare Ti foil, and Pt mesh electrode. (b) Corresponding Tafel plots for the Ni_2P nanocrystal and Pt mesh electrodes.

data for the Ni₂P nanocrystals, along with a standard Pt mesh electrode and a bare Ti foil as working electrodes. The Ni₂P nanocrystals exhibited overpotentials of $\eta_{-10\text{mA/cm}^2} = -107 \text{ mV}$ and $\eta_{-20\text{mA/cm}^2} = -125 \text{ mV}$, as compared to the overpotentials for the Pt mesh electrode ($\eta_{-10 {\rm mA/cm}^2}$ = -12 mV and $\eta_{-20 {\rm mA/cm}^2}$ = -20 mV). The bare Ti foil substrate did not exhibit substantial electrocatalytic activity for HER over this potential range. The Tafel slopes were 30 and 70 mV/decade for Pt mesh and the Ni₂P nanocrystals, respectively. These overpotentials and Tafel slopes are in accord with the behavior of Ni₂P nanocrystal-based electrodes with comparable mass loadings that were synthesized using typical high-boiling organic solvents.³³ For example, Schaak and co-workers reported an overpotential and Tafel slope of $\eta_{-10\text{mA/cm}^2}$ = -116 mV and 46 mV/decade for their Ni₂P nanocrystals synthesized in ODE using similar reagents. 10 Galvanostatic measurements at a current density of -20 mA/cm² displayed only a slight decrease in potential over the course of 15 h of continuous hydrogen evolution (Figure S5). Cyclic voltammogram sweeps of the Ni₂P electrode between 0 and -0.2 V vs RHE illustrate the continued activity of the nanocrystals during on and off cycling (Figure S6). Moreover, chronopotentiometric measurements for the Ni₂P nanocrystals in 1 M NaOH showed that they also exhibit stable operation in alkaline media at -10 mA/cm^2 for more than 10 h (Figure S7).

The synthetic methodology described herein was also extended to the synthesis of phase-pure, mixed-metal $Ni_{2-x}Co_xP$ nanocrystals $(0.5 \le x \le 1.5)$ by simply adjusting the precursor ratio of $Ni(acac)_2$ to $Co(acac)_2$ and increasing the reaction time (see Supporting Information for detailed experimental and characterization). The resulting nanocrystals

display a similar size to the Ni_2P nanocrystals (Figure S8); however, as the concentration of Co increased, the nanocrystals became gradually more faceted and morphologically dissimilar, which has been previously observed for Co-rich $Ni_{2-x}Co_xP$ structures. ^{11,34}

The composition of the mixed-metal Ni_{2-x}Co_xP nanocrystals was confirmed through a combination of XRD, XPS, and energy dispersive X-ray (EDS) analyses. As the Co content increased, the powder XRD patterns showed a decrease in intensity of the (201) and (210) reflections, and the peak envelope of the (300) and (211) reflections at $\sim 54^{\circ}$ 2 θ that appeared as a single peak for $x \le 1.0$ split into two resolvable peaks, corresponding to the (002) and (320) reflections of the bulk orthorhombic Co_2P structure, for x = 1.5 (Figure S9). The unit cell volume increased linearly with increasing Co content for the hexagonal structure (x = 0, 0.5, 1.0), confirming that the material was a homogeneous solid solution (Figure S10). The experimentally determined composition determined from highresolution XPS scans of the Ni and Co 2p regions were in close accord with the nominal compositions used during synthesis, indicating facile Co incorporation within the 1 h reaction time (Table S1). The nanocrystals with a Ni_{1.0}Co_{1.0}P nominal composition were further examined by EDS mapping, which corroborated that the nominal composition matched the experimental composition and that the Co and Ni were homogeneously distributed over a cluster of nanocrystals (Figure S12).

In summary, small, phase-pure Ni_2P nanocrystals can be synthesized using the IL solvent, BMIM-Tf₂N. Under analogous reaction conditions, substituting ODE for the IL instead produced ill-defined, phase-impure nanocrystals, suggesting that the IL plays an important role in the reaction. XPS and FT-IR spectroscopic evidence confirmed coordination of the IL to the nanocrystal surface. Despite surface coordination of the IL, the resulting nanocrystals displayed comparable HER activity to Ni_2P nanocrystals synthesized by other routes.

ASSOCIATED CONTENT

S Supporting Information

The Supporting Information is available free of charge on the ACS Publications website at DOI: 10.1021/acsaem.8b00213.

Experimental details, TGA trace of Ni_2P , TEM micrograph of nanocrystals produced in ODE, additional XPS spectra of Ni_2P , FT-IR spectrum of Ni_2P , additional electrochemical measurements for Ni_2P , TEM images, and XRD and XPS data for $Ni_{2-x}Co_xP$ nanocrystals (PDF)

AUTHOR INFORMATION

Corresponding Authors

*E-mail: nslewis@caltech.edu. *E-mail: brutchey@usc.edu.

ORCID ®

Nathan S. Lewis: 0000-0001-5245-0538 Richard L. Brutchey: 0000-0002-7781-5596

Notes

The authors declare no competing financial interest.

ACKNOWLEDGMENTS

R.L.B. acknowledges NSF for supporting the synthetic chemistry under CMMI-1728649. N.S.L. acknowledges NSF for supporting the electrochemical characterization work under the NSF CCI Solar Fuels Program CHE-1305124. C.G.R. acknowledges the Resnick Sustainability Institute for a postdoctral fellowship.

ABBREVIATIONS

acetylacetonate, acac 1-butyl-3-methylimidazolium bis(trifluoromethylsulfonyl)-imide, BMIM- Tf_2N ionic liquid, IL 1-octadecene, ODE oleylamine, OAm trioctylphosphine, TOP triphenylphosphine, PPh_3

REFERENCES

- (1) Wasserscheid, P.; Welton, T. *Ionic Liquids in Synthesis*; John Wiley & Sons, 2008.
- (2) Dupont, J.; Suarez, P. A. Z. Physico-Chemical Processes in Imidazolium Ionic Liquids. *Phys. Chem. Chem. Phys.* **2006**, *8*, 2441–2452.
- (3) Lazarus, L. L.; Riche, C. T.; Marin, B. C.; Gupta, M.; Malmstadt, N.; Brutchey, R. L. Two-Phase Microfluidic Droplet Flows of Ionic Liquids for the Synthesis of Gold and Silver Nanoparticles. *ACS Appl. Mater. Interfaces* **2012**, *4*, 3077–3083.
- (4) Riche, C. T.; Roberts, E. J.; Gupta, M.; Brutchey, R. L.; Malmstadt, N. Flow Invariant Droplet Formation for Stable Parallel Microreactors. *Nat. Commun.* **2016**, *7*, 10780.
- (5) Kunal, P.; Roberts, E. J.; Riche, C. T.; Jarvis, K.; Malmstadt, N.; Brutchey, R. L.; Humphrey, S. M. Continuous Flow Synthesis of Rh and RhAg Alloy Nanoparticle Catalysts Enables Scalable Production and Improved Morphological Control. *Chem. Mater.* **2017**, *29*, 4341–4350.
- (6) Kessler, M. T.; Hentschel, M. K.; Heinrichs, C.; Roitsch, S.; Prechtl, M. H. G. Fast Track to Nanomaterials: Microwave Assisted Synthesis in Ionic Liquid Media. RSC Adv. 2014, 4, 14149–14156.
- (7) Meine, N.; Benedito, F.; Rinaldi, R. Thermal Stability of Ionic Liquids Assessed by Potentiometric Titration. *Green Chem.* **2010**, *12*, 1711–1714.
- (8) Wagle, D. V.; Rondinone, A. J.; Woodward, J. D.; Baker, G. A. Polyol Synthesis of Magnetite Nanocrystals in a Thermostable Ionic Liquid. *Cryst. Growth Des.* **2017**, *17*, 1558–1567.
- (9) Habas, S. E.; Baddour, F. G.; Ruddy, D. A.; Nash, C. P.; Wang, J.; Pan, M.; Hensley, J. E.; Schaidle, J. A. A Facile Molecular Precursor Route to Metal Phosphide Nanoparticles and Their Evaluation as Hydrodeoxygenation Catalysts. *Chem. Mater.* **2015**, *27*, 7580–7592.
- (10) Popczun, E. J.; McKone, J. R.; Read, C. G.; Biacchi, A. J.; Wiltrout, A. M.; Lewis, N. S.; Schaak, R. E. Nanostructured Nickel Phosphide as an Electrocatalyst for the Hydrogen Evolution Reaction. *J. Am. Chem. Soc.* **2013**, *135*, 9267–9270.
- (11) Callejas, J. F.; Read, C. G.; Popczun, E. J.; McEnaney, J. M.; Schaak, R. E. Nanostructured Co₂P Electrocatalyst for the Hydrogen Evolution Reaction and Direct Comparison with Morphologically Equivalent CoP. *Chem. Mater.* **2015**, *27*, 3769–3774.
- (12) Li, D.; Senevirathne, K.; Aquilina, L.; Brock, S. L. Effect of Synthetic Levers on Nickel Phosphide Nanoparticle Formation: Ni₅P₄ and NiP₂. *Inorg. Chem.* **2015**, *54*, 7968–7975.
- (13) Muthuswamy, E.; Savithra, G. H. L.; Brock, S. L. Synthetic Levers Enabling Independent Control of Phase, Size, and Morphology in Nickel Phosphide Nanoparticles. *ACS Nano* **2011**, *5*, 2402–2411.
- (14) Liu, J.; Meyns, M.; Zhang, T.; Arbiol, J.; Cabot, A.; Shavel, A. Triphenyl Phosphite as the Phosphorous Source for the Scalable and Cost-Effective Production of Transition Metal Phosphides. *Chem. Mater.* **2018**, *30*, 1799–1807.

ACS Applied Energy Materials

- (15) Carenco, S.; Resa, I.; Le Goff, X.; Le Floch, P.; Mézailles, N. White Phosphorus as Single Source of "P" in the Synthesis of Nickel Phosphide. *Chem. Commun.* **2008**, 2568–2570.
- (16) Perera, S. C.; Fodor, P. S.; Tsoi, G. M.; Wenger, L. E.; Brock, S. L. Application of De-Silylation Strategies to the Preparation of Transition Metal Pnictide Nanocrystals: The Case of FeP. *Chem. Mater.* **2003**, *15*, 4034–4038.
- (17) Wang, J.; Johnston-Peck, A. C.; Tracy, J. B. Nickel Phosphide Nanoparticles with Hollow, Solid, and Amorphous Structures. *Chem. Mater.* **2009**, 21, 4462–4467.
- (18) Zafiropoulou, I.; Papagelis, K.; Boukos, N.; Siokou, A.; Niarchos, D.; Tzitzios, V. Chemical Synthesis and Self-Assembly of Hollow Ni/Ni2P Hybrid Nanospheres. *J. Phys. Chem. C* **2010**, *114*, 7582–7585.
- (19) Zheng, X.; Yuan, S.; Tian, Z.; Yin, S.; He, J.; Liu, K.; Liu, L. One-Pot Synthesis of Hollow Nickel Phosphide Nanoparticles with Tunable Void Sizes Using Triphenylphosphine. *Mater. Lett.* **2009**, 63, 2283–2285.
- (20) Pan, Y.; Liu, Y.; Liu, C. An Efficient Method for the Synthesis of Nickel Phosphide Nanocrystals via Thermal Decomposition of Single-Source Precursors. *RSC Adv.* **2015**, *5*, 11952—11959.
- (21) Chiang, R.-K.; Chiang, R.-T. Formation of Hollow Ni₂P Nanoparticles Based on the Nanoscale Kirkendall Effect. *Inorg. Chem.* **2007**, *46*, 369–371.
- (22) Dupont, J.; Scholten, J. D. On the Structural and Surface Properties of Transition-Metal Nanoparticles in Ionic Liquids. *Chem. Soc. Rev.* **2010**, *39*, 1780–1804.
- (23) Essig, S.; Behrens, S. Ionic Liquids as Size- and Shape-Regulating Solvents for the Synthesis of Cobalt Nanoparticles. *Chem. Ing. Tech.* **2015**, 87, 1741–1747.
- (24) Gutel, T.; Santini, C. C.; Philippot, K.; Padua, A.; Pelzer, K.; Chaudret, B.; Chauvin, Y.; Basset, J.-M. Organized 3D-Alkyl Imidazolium Ionic Liquids Could Be Used to Control the Size of in Situ Generated Ruthenium Nanoparticles? *J. Mater. Chem.* **2009**, *19*, 3624–3631.
- (25) Redel, E.; Thomann, R.; Janiak, C. First Correlation of Nanoparticle Size-Dependent Formation with the Ionic Liquid Anion Molecular Volume. *Inorg. Chem.* **2008**, *47*, 14–16.
- (26) Moreau, L. M.; Ha, D.-H.; Zhang, H.; Hovden, R.; Muller, D. A.; Robinson, R. D. Defining Crystalline/Amorphous Phases of Nanoparticles through X-Ray Absorption Spectroscopy and X-Ray Diffraction: The Case of Nickel Phosphide. *Chem. Mater.* **2013**, *25*, 2394–2403.
- (27) Andaraarachchi, H. P.; Thompson, M. J.; White, M. A.; Fan, H. J.; Vela, J. Phase-Programmed Nanofabrication: Effect of. Organophosphite Precursor Reactivity on the Evolution of Nickel and Nickel Phosphide Nanocrystals. *Chem. Mater.* **2015**, *27*, 8021–8031.
- (28) Pan, Y.; Liu, Y.; Zhao, J.; Yang, K.; Liang, J.; Liu, D.; Hu, W.; Liu, D.; Liu, Y.; Liu, C. Monodispersed Nickel Phosphide Nanocrystals with Different Phases: Synthesis, Characterization and Electrocatalytic Properties for Hydrogen Evolution. *J. Mater. Chem. A* **2015**, *3*, 1656–1665.
- (29) Biesinger, M. C.; Payne, B. P.; Lau, L. W. M.; Gerson, A.; Smart, R. S. C. X-Ray Photoelectron Spectroscopic Chemical State Quantification of Mixed Nickel Metal, Oxide and Hydroxide Systems. Surf. Interface Anal. 2009, 41, 324–332.
- (30) Li, D.; Arachchige, M. P.; Kulikowski, B.; Lawes, G.; Seda, T.; Brock, S. L. Control of Composition and Size in Discrete Co_xFe_{2-x}P Nanoparticles: Consequences for Magnetic Properties. *Chem. Mater.* **2016**, 28, 3920–3927.
- (31) Rey, I.; Johansson, P.; Lindgren, J.; Lassègues, J. C.; Grondin, J.; Servant, L. Spectroscopic and Theoretical Study of $(CF_3SO_2)_2N^-$ (TFSI⁻) and $(CF_3SO_2)_2NH$ (HTFSI). *J. Phys. Chem. A* **1998**, *102*, 3249–3258.
- (32) Clark, R. J. H.; Flint, C. D.; Hempleman, A. J. F.T.I.R. and Raman Spectra of Triphenylphosphine, Triphenylarsine, Triphenylstibine, and Dibenzylsulphide. *Spectrochim. Acta Part Mol. Spectrosc.* 1987, 43, 805–816.
- (33) Callejas, J. F.; Read, C. G.; Roske, C. W.; Lewis, N. S.; Schaak, R. E. Synthesis, Characterization, and Properties of Metal Phosphide

- Catalysts for the Hydrogen-Evolution Reaction. Chem. Mater. 2016, 28, 6017-6044.
- (34) Liyanage, D. R.; Danforth, S. J.; Liu, Y.; Bussell, M. E.; Brock, S. L. Simultaneous Control of Composition, Size, and Morphology in Discrete Ni_{2-x}Co_xP Nanoparticles. *Chem. Mater.* **2015**, *27*, 4349–4357.